THE JOURNAL OF PHYSICAL CHEMISTRY C
A JOURNAL OF THE AMERICAN CHEMICAL SOCIETY

pubs.acs.org/JPCC

Article

Unraveling the SO_2 Poisoning Effect over the Lifetime of MeO_x (Me = Ce, Fe, Mn) Catalysts in Low-Temperature NH_3-SCR: Interaction of Reaction Atmosphere with Surface Species

Dongqi An, Shan Yang, Weixin Zou, Jingfang Sun,* Wei Tan, Jiawei Ji, Qing Tong, Chuanzhi Sun, Dan Li,* and Lin Dong

Cite This: *J. Phys. Chem. C* 2022, 126, 12168−12177

Read Online

ACCESS | Metrics & More | Article Recommendations | Supporting Information

ABSTRACT: A fundamental understanding of the effect of SO_2 on low-temperature NH_3-SCR is vitally important for SO_2-tolerant catalysts. Here, the effects of SO_2 on CeO_2, γ-Fe_2O_3, and γ-MnO_2 were reported, and the mechanism was thoroughly elucidated. Based on the experimental and density functional theory study, it was discovered that the NH_3-SCR performance of different metal oxide catalysts in a sulfur-containing atmosphere was closely related to the difference in the deposition/decomposition ability of the formed sulfate species. For CeO_2 and γ-Fe_2O_3, corresponding metal sulfates governed their denitrification efficiency when facing SO_2 intrusion, favored by the equilibrium between deposition and consumption of surface ammonium bisulfate. However, the activity of γ-MnO_2, hardly affected by the formed manganese sulfate, was mainly encroached by a large amount of ABS covering active sites. Meanwhile, NH_3, the reducing agent in the gas phase, significantly boosted the decomposition of metal sulfates. Moreover, the most easily decomposed iron sulfate, thus, claimed responsibility for the long-lasting sulfur tolerance of γ-Fe_2O_3.

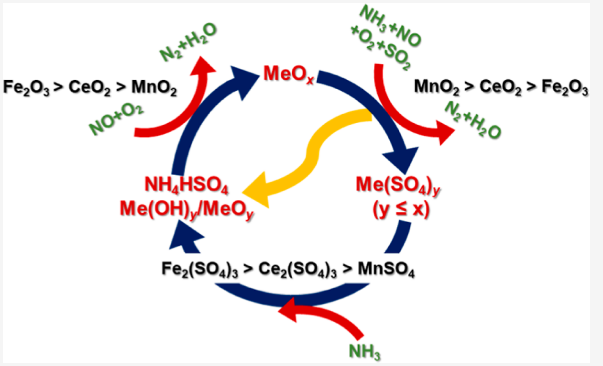

1. INTRODUCTION

Selective catalytic reduction of nitrogen oxides (NO_x) with NH_3 (NH_3-SCR) is an efficient technology for NO_x elimination.[1,2] As the currently most widely used NH_3-SCR industrial catalyst, V_2O_5-$WO_3(MoO_3)$/TiO_2 (VWTi) still has several unavoidable shortcomings, for example, an unsatisfactory low-temperature catalytic performance, a relatively narrow operation temperature window (300−400 °C), and toxicity of V_2O_5, which restrict its further practical application.[3−6] Especially with the increasing demand for flue gas deNO_x in nonpower industries (such as steel sintering machines, glass furnaces, and cement furnaces), the lower flue gas temperature (100−280 °C)[7] makes it difficult to match the use of VWTi catalysts. Therefore, whether from the perspective of energy saving (flue gas is heated first and then denitrified in many industries) or environment protection (V_2O_5 is toxic), it's urgent to develop eco-friendly low-temperature NH_3-SCR catalysts with high efficiency.

In recent years, more and more research focuses on Mn-based,[8−11] Fe-based,[12−15] and Ce-based[16,17] catalysts. The elements Mn, Fe, and Ce existing either as a support or a modifier make the catalysts not only exhibit an excellent low-temperature activity but also show certain sulfur tolerance. However, it should be noted that the current research on the nature of low-temperature performance improvement is going deeper but leaves the mechanism of sulfur tolerance awaiting some rational elaboration. Owing to the complexity of catalysts and the sulfur-containing reaction, the contribution of specific elements is difficult to define, and the nature of SO_2 tolerance is easily confused. Particularly, the complexity of the research on the sulfur tolerance of catalysts is reflected in two aspects: (1) the diversity of sulfur-containing species (ABS, ammonium sulfate, and metal sulfates of different valences, etc.) and the different poisoning effects of these species in a specific catalyst system; (2) the intricacy of catalyst components (a variety of metal elements contained) leading to the different states and content of sulfur-containing species.

For example, Yu et al.[18] found that the NO conversion of the Ce/MnO_x/SAPO-34 catalyst kept decreasing after SO_2 was introduced, and the ABS formed was proved to lead to a continuous deactivation by covering the active sites. While Gan et al.[19] observed that the generation of a large amount of

Received: April 4, 2022
Revised: June 29, 2022
Published: July 14, 2022

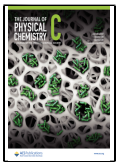

https://doi.org/10.1021/acs.jpcc.2c02233
J. Phys. Chem. C 2022, 126, 12168−12177

$MnSO_3/MnSO_4$ was identified as the main reason for the persistent decrease in the activity of α-MnO_2 and Ce/α-MnO_2 with SO_2, a deactivation caused by the sulfation of the active component. Apparently, no unanimous conclusion can be drawn even in the discussion of the SO_2 tolerance of the same component. Furthermore, the role of the same component would be quite different in various multicomponent systems. Ye et al.[20] reported that after adding Fe to the Ce/Nb catalyst, its SO_2 tolerance was significantly improved. Relevant experimental characterization demonstrated that SO_4^{2-} was easier to combine with the addition of Fe, protecting the main active component Ce from sulfation. However, Yu et al.[18] claimed Ce served as a sacrificial agent, giving priority to be sulfated and thus retaining the Mn active sites. Also, Xie et al.[21] found that Ce-doped γ-Fe_2O_3 had an excellent anti-SO_2 oxidation performance, which restrained the formation of sulfates. These phenomena seemed to indicate that simplifying catalyst components or comparative studies based on controlled variables were the inevitable approaches to exploring the mechanism of SO_2 tolerance.

Fortunately, some inspiration was acquired from published works. Fan et al.[22] found that the content and thermal stability of sulfates species were different through loading of Al_2O_3 and other 20 kinds of single-metal oxides, respectively, on MnO_x to improve its SO_2 tolerance. The Al_2O_3 additive proved to be optimum in boosting the decomposition of ABS and inhibiting the reaction between MnO_x and SO_2. Wang et al.[23] discovered that S-containing species affected the catalytic activity by blocking NH_3/NO adsorption. Also, the sulfate species decomposed more easily on the poisoned FeW/Ti catalyst through comparative research, preceding other MW/Ti catalysts (M = Fe, Mn, Cu, and V). Nevertheless, the specific mechanism of sulfate species on each component is still unclear. Therefore, further component simplifications, such as building model catalysts and a comparative study on this basis, are indispensable. Just recently, He et al.[24] have taken the lead in adopting this research ideology. Through theoretical calculations and comparative studies, they answered the essential reason for the excellent low-temperature activity of Mn-based catalysts.

Hence, three catalysts, CeO_2, γ-Fe_2O_3, and γ-MnO_2,[19,25,26] were chosen as representatives for their completely different sulfur tolerance. Afterward, a series of characterization methods were implemented to explore the mechanism in detail. Also, the SO_2 poisoning effect over the lifetime of metal oxide catalysts was expressly clarified by revealing the interactions at the interface in the whole catalytic reaction system in this work.

2. EXPERIMENTAL SECTION

2.1. Catalyst Synthesis. *2.1.1. CeO_2.* CeO_2 was prepared by the thermal decomposition of $Ce(NO_3)_3{\cdot}6H_2O$ at 550 °C for 4 h in air.

2.1.2. γ-Fe_2O_3. γ-Fe_2O_3 was prepared by a co-precipitation method. First, $FeSO_4{\cdot}7H_2O$ (12.5 mmol) and $FeCl_3{\cdot}6H_2O$ (25 mmol) were dissolved in deionized water (250 mL), and 150 mL of the ammonia (1 mol·L^{-1}) solution was then added dropwise to the solution with continuous stirring for 2 h, followed by filtering. The solid obtained was washed with distilled water, dried at 80 °C overnight, and calcined at 300 °C in air for 3 h to give γ-Fe_2O_3.

2.1.3. γ-MnO_2. γ-MnO_2 was prepared by a hydrothermal method. First, $MnSO_4{\cdot}H_2O$ (20 mmol) and $(NH_4)_2{\cdot}S_2O_8$ (20 mmol) were dissolved in deionized water (80 mL) with continuous stirring for 2 h. Then, the mixed solution was transferred into a 100 mL Teflon-lined stainless-steel autoclave and heated at 90 °C for 24 h, followed by filtering. The solid obtained was washed with distilled water, dried at 80 °C overnight, and calcined at 350 °C in air for 3 h to give γ-MnO_2.

2.1.4. Samples after In Situ Sulfur Tolerance for Different Times. CeO_2, γ-Fe_2O_3, and γ-MnO_2 prepared withstood sulfur tolerance test at 250 °C for 2, 5, and10 h, respectively. The inlet gas was 500 ppm NO, 500 ppm NH_3, 5 vol % O_2, and 100 ppm SO_2, and the total gas flow rate was 200 mL/min. The obtained samples were denoted as Me-p-2/5/10 h (Me = Ce, Fe, and Mn).

2.1.5. Samples Containing Metal Sulfates Only. Me-p-2/5/10 h were purged at 350 °C under an Ar atmosphere for 1 h to remove the ABS presented on the surface. The obtained samples were denoted as Me-p-2/5/10 h-350 (Me = Ce, Fe, and Mn).

2.1.6. SO_2 + O_2 Pretreated γ-MnO_2 Samples. γ-MnO_2 was pretreated with 100 ppm SO_2 + 5 vol % O_2 with Ar as the balance gas at 250 °C for 2, 5, and 10 h to simulate the situation where only metal sulfates were presented. The obtained samples were denoted as Mn-s-2/5/10 h.

2.2. Characterizations. X-ray diffraction (XRD) patterns were recorded on a Philips X'pert Pro diffractometer using Ni-filtered Cu Kα radiation (λ = 0.15418 nm) from 10 to 80°. The X-ray tube was operated at 40 kV and 30 mA.

Fourier transform infrared (FT-IR) spectra were collected on a Nicolet IS10 FT-IR spectrometer at a spectral resolution of 4 cm^{-1} for 32 scans. The background was collected first and then subtracted for every sample.

Ion chromatography (IC) was used to detect soluble species on samples. The content of ABS and metal sulfates were inferred based on the quantitatively analyzed NH_4^+ and SO_4^{2-} in the samples after the sulfur tolerance test. The samples with 25 mg, respectively, were dispersed in 24.85 mL of deionized water and 0.15 mL of nitric acid solution at 16 mol·L^{-1} and placed overnight. Then, the solutions were filtered with a 0.22 μm filter membrane, and the liquid phases were prepared for the IC tests.

Thermogravimetry (TG) was conducted on NETZSCH sta-449-F5. The samples were heated under a flow of nitrogen atmosphere (60 mL/min) with a heating rate of 10 °C·min^{-1} from room temperature to 900 °C. The reference TG curve was obtained by operating the same analysis on an empty crucible.

Temperature-programmed surface reaction (TPSR) experiments were performed with a Nicolet IS10 FTIR spectrometer and an online LC-D series mass spectrometer. First, the Me-p-5 h sample (100 mg) was loaded into a quartz tube and exposed to 500 ppm NO + 5 vol % O_2 or 500 ppm NH_3 (gas mixture of 100 mL/min, Ar balanced) until saturation at ambient temperature. After that, the sample was heated up to 730/250 °C at a rate of 10 °C·min^{-1} to record the NO and N_2 signal.

Temperature-programmed desorption (TPD) measurements were carried out in a fixed-bed quartz reactor equipped with an FTIR spectrometer to monitor the outlet gas signal, and the interval of spectrum collection was set at 30 s. For the NH_3/NO-TPD experiment, 50 mg of Me-p-5h-350 sample was exposed to 500 ppm NH_3 or 500 ppm NO + 5 vol % O_2 (gas mixture of 50 mL/min, Ar balanced) until saturation at ambient temperature. Subsequently, the sample was purged

https://doi.org/10.1021/acs.jpcc.2c02233
J. Phys. Chem. C 2022, 126, 12168−12177

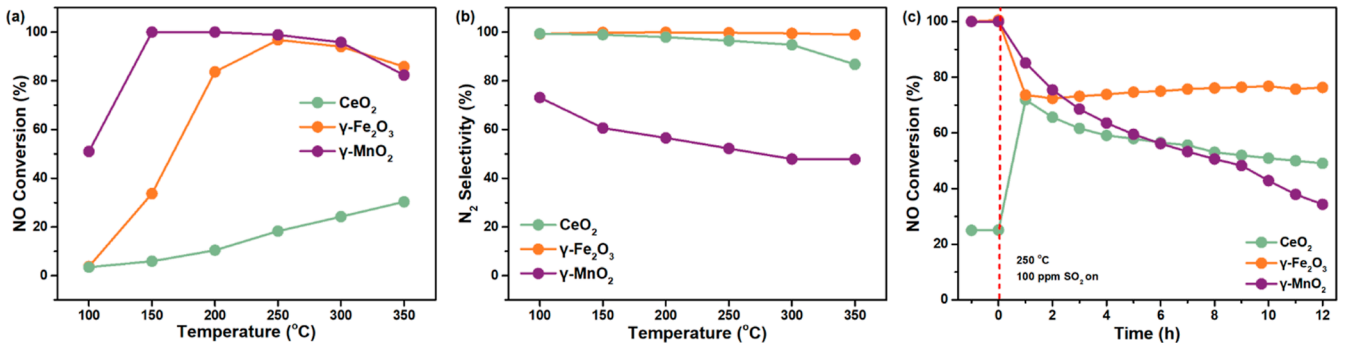

Figure 1. (a) NO conversion and (b) N_2 selectivity of CeO_2, γ-Fe_2O_3, and γ-MnO_2 as a function of the reaction temperature. (c) Sulfur tolerance tests on CeO_2, γ-Fe_2O_3, and γ-MnO_2 in the presence of 100 ppm SO_2 as a function of the reaction time (the feeding gas contained 500 ppm NH_3, 500 ppm NO, 5% O_2. WHSV = 60 000 mL·g^{-1}·h^{-1}.).

with flowing highly purified Ar to remove gaseous and weakly absorbed species. Finally, the sample was heated to 650 °C at a rate of 10 °C·min^{-1} to record the NH_3 or NO signal. For the SO_2-TPD experiment, 50 mg of CeO_2/γ-Fe_2O_3/γ-MnO_2 sample was exposed to SO_2 + 5 vol % O_2 (gas mixture of 50 mL/min, Ar balanced) until saturation at 250 °C. Subsequently, the sample was purged with flowing highly purified Ar to remove gaseous and weakly absorbed species. Finally, the sample was heated to 730 °C at a rate of 10 °C·min^{-1} to record the SO_2 signal.

In situ DRIFTS experiments were conducted on a Nicolet Nexus 5700 FTIR spectrometer. The spectra were collected by an MCT detector and presented as a Kubelka−Munk function. The resolution was 4 cm^{-1}, and 32 scans were taken. Before collecting the background spectra, the powder samples were pretreated with highly purified N_2 at 400 °C (for CeO_2) or 300 °C (for γ-Fe_2O_3 and γ-MnO_2) for 0.5 h. Background spectra were then collected in a flowing highly purified N_2 stream as the powder samples cooled to 250 °C. The sample spectra were then obtained after the subtraction of the background spectra. The samples were exposed to a controlled stream of a specific gas mixture for a certain amount of time: 3000 ppm NH_3; 500 ppm SO_2 + 5 vol % O_2; 3000 ppm NO + 5 vol % O_2; 3000 ppm NH_3 + 3000 ppm NO + 5 vol % O_2. All of the reaction gasses were balanced with N_2 at a flow rate of 50 mL/min.

2.3. Catalytic Performance Tests. The SCR activity tests were carried out in a fixed-bed quartz tube reactor, and the reaction gas contained 500 ppm NO, 500 ppm NH_3, 5 vol % O_2, 100 ppm SO_2 (when used), and Ar in balance. The total gas flow rate was 200 mL/min, corresponding to a weight hourly space velocity (WHSV) of 60 000 mL·g^{-1}·h^{-1}. Prior to the test, flaky samples (obtained from catalyst powder after being compressed, ground, and sieved into 40−60 mesh particles.) of 200 mg underwent a pure Ar stream pretreatment at 200 °C for 0.5 h to remove the moisture and impurities and then cooled to ambient temperature. After that, the reaction system was introduced with the gas mixture, and the reaction activity data was collected at each target temperature. The concentrations of outlet gases were detected by an online Nicolet IS10 FTIR spectrometer. NO conversion and N_2 selectivity were calculated according to the following formulas, respectively

$$\text{NO conversion} = \frac{[\text{NO}]_{\text{in}} - [\text{NO}]_{\text{out}}}{[\text{NO}]_{\text{in}}} \times 100\% \quad (1)$$

$$N_2\ \text{selectivity} = 100\% \times \{[\text{NO}]_{\text{in}} - [\text{NO}]_{\text{out}} + [\text{NH}_3]_{\text{in}} - [\text{NH}_3]_{\text{out}} - [\text{NO}_2]_{\text{out}} - 2[\text{N}_2\text{O}]_{\text{out}}\}/\{[\text{NO}]_{\text{in}} - [\text{NO}]_{\text{out}} + [\text{NH}_3]_{\text{in}} - [\text{NH}_3]_{\text{out}}\} \quad (2)$$

The details of density functional theory theoretical calculation could be found in the Supporting Information.

3. RESULTS AND DISCUSSION

3.1. Catalytic Performance and the Sulfur Tolerance Test. The XRD spectra of the target catalysts were displayed in Figure S1, and all samples were in line with the crystal structure we designed. The NO conversion and N_2 selectivity of CeO_2, γ-Fe_2O_3, and γ-MnO_2 were shown in Figure 1a,b. It can be found that the three samples presented totally different catalytic activity curves. CeO_2 showed a poor catalytic activity with the highest NO conversion of only 40%, and this was why it usually served as a support or adjuvant. Although the catalytic performance of γ-Fe_2O_3 below 200 °C was unsatisfactory, it maintained an NO conversion over 80% at 200−350 °C. However, the consistency of the two lies in the superior N_2 selectivity in the entire temperature range, close to 100%. As γ-MnO_2 displayed an inferior N_2 selectivity, over 80% NO conversion at 150−350 °C was performed simultaneously. A favorable activity made γ-Fe_2O_3 and γ-MnO_2 be regarded as the preferred active components for low-temperature NH_3-SCR catalysts. Taking into account the flue gas temperature in the nonelectric industry and the decreased activity of conventional catalysts after sulfurization, 250 °C was chosen as the temperature to study the trend of sulfur tolerance of different catalysts.

As shown in Figure 1c, CeO_2, γ-Fe_2O_3, and γ-MnO_2 represented different sulfur tolerance after 100 ppm SO_2 was introduced: (1) the activity of CeO_2 increased rapidly in the first 1 h, with a NO conversion up to 70%, and then gradually decreased with the time on. Zhang et al.,[27] in our group, declared that the surface sulfates gave an enhanced activity to CeO_2 by increasing its acidity, while the bulk sulfates brought by the deepened sulfation process impaired its activity. (2) Contrary to the performance of CeO_2, the NO conversion of γ-Fe_2O_3 dropped suddenly from 100 to 70% within 1 h after the introduction of SO_2 and then remained at about 70%, showing a slow upward trend over time. Yu et al.[26] believed that this phenomenon was mainly attributed to the changes in the surface sulfate species before and after the sulfurization and the resulting changes in the reaction pathway. (3) For γ-MnO_2, a

https://doi.org/10.1021/acs.jpcc.2c02233
J. Phys. Chem. C 2022, 126, 12168−12177

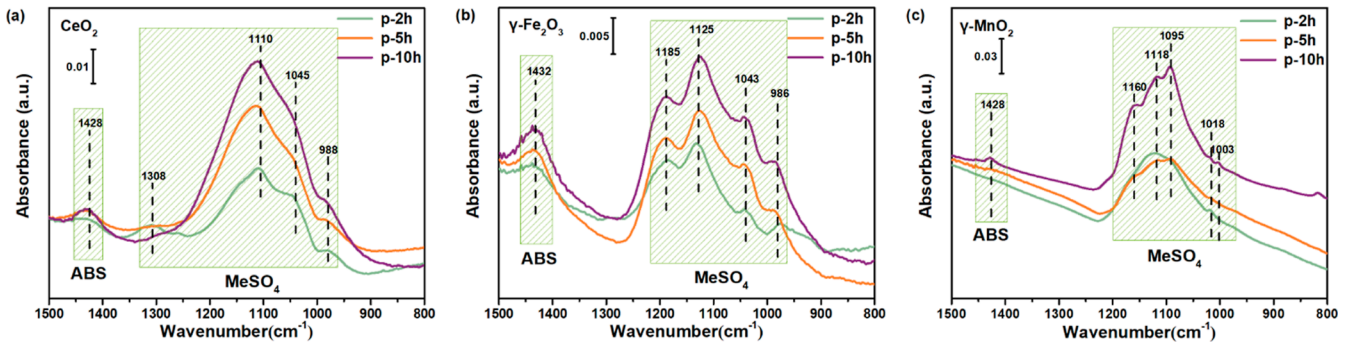

Figure 2. IR spectra of (a) Ce-p-2/5/10 h, (b) Fe-p-2/5/10 h, and (c) Mn-p-2/5/10 h.

constant decline in its NO conversion spread out with the continuously introduced SO_2. As discussed before,[28,29] the perception of sulfur tolerance of manganese oxide was still uncompromising, entangled by ABS domination or metal sulfate domination. It can be inferred that though certain conclusions gained, the essential reason why different oxides performed diverse sulfur tolerance remains unknown. Building on past achievements and striving for new progress, the key factors, catalysts, ABS, metal sulfates, and their reaction atmosphere, become the focus of our discussion in the following research.

3.2. Surface Sulfate Species Clarification. Determining the existence state of sulfate species is a prerequisite for analyzing the influence on the sulfur tolerance of the catalyst. FT-IR is skilled in differentiating various S-containing species and is sensitive to the NH_4^+ in ABS. Hence, IR spectra of Me-p-2/5/10 h were performed, and the results are shown in Figure 2a–c. The sulfation process of CeO_2, γ-Fe_2O_3, and γ-MnO_2 gradually deepened with sulfur tolerance time, demonstrating the accumulation of ABS and metal sulfates and the final appearance of bulk sulfates. Universally, bands assigned to NH_4^+ in ABS (1428 cm^{-1} for Ce-p-2/5/10 h, 1432 cm^{-1} for Fe-p-2/5/10 h, and 1428 cm^{-1} for Mn-p-2/5/10 h) were all observed on the surface of the samples.[30] Beyond that, sulfate species including S–O species (1110 cm^{-1} for Ce-p-2/5/10 h, 1125 cm^{-1} for Fe-p-2/5/10 h, and 1118, 1095, 1018, 1003 cm^{-1} for Mn-p-2/5/10 h), S=O species (1308 cm^{-1} for Ce-p-2/5/10 h), and bulk sulfate species (1045, 988 cm^{-1} for Ce-p-2/5/10 h, 1185, 1043, 986 cm^{-1} for Fe-p-2/5/10 h, and 1160 cm^{-1} for Mn-p-2/5/10 h) are also presented.[27]

Aiming to further determine the precise content of each sulfate species, the pickling Me-p-2/5/10 h were then subjected to IC with the ion concentration (ppm) and corresponding wt % listed in Table 1. Taking the negligible experimental errors and other factors into account, it can be found that the content of both sulfate species increased with the sulfur tolerance test time. In particular, the amount of surface ABS on γ-MnO_2 increased rapidly during the 5–10 h, in contrast with the slow accumulation on CeO_2 and γ-Fe_2O_3. Ma et al.[31] once reported that the amount of surface ABS was constant and did not accumulate on CeO_2 even if it was tested in the presence of SO_2 for 1000 h. Same for γ-Fe_2O_3, Yu et al.[26] found that the content of ABS on γ-Fe_2O_3 changed little even up to 216 h. Both studies confirmed the establishment of a dynamic equilibrium between deposition and consumption of ABS on CeO_2 and γ-Fe_2O_3. As for metal sulfates, a slackened increase rate with time was another puzzle to be solved later. Additionally, TG curves gave a further demonstration of the thermal stability of surface sulfates (Figure S2). Except for

Table 1. Ion Concentration of the Pickling Ce-p-2/5/10 h, Fe-p-2/5/10 h, and Mn-p-2/5/10 h Samples at 250 °C

	ion concentration (ppm)			
catalyst	ABS	metal sulfate	$m_{ABS}/m_{cat.}$ (wt %)	$m_{metal\ sulfate}/m_{cat.}$ (wt %)
Ce-p-2 h	2.2	1.3	0.44	0.26
Ce-p-5 h	2.8	18.7	0.56	3.74
Ce-p-10 h	3.4	30.1	0.68	6.02
Fe-p-2 h	2.3	8.1	0.46	1.62
Fe-p-5 h	2.8	15.6	0.56	3.12
Fe-p-10 h	2.7	29.8	0.54	5.96
Mn-p-2 h	2.9	47.1	0.58	9.42
Mn-p-5 h	3.1	69.1	0.62	13.8
Mn-p-10 h	5.1	83.1	1.02	16.6

weight loss corroborating the IC results, it showed that ABS could start to decompose at about 250 °C, and the decomposition temperature of each metal sulfate was quite different, which could be attributed to the decomposition of $Ce_2(SO_4)_3$,[31,32] $Fe_2(SO_4)_3$[33] and $MnSO_4$.[23] To sum up, in view of the differences in the content of sulfate species on Me-p-2/5/10 h, it's worth studying how each sulfate species evolved over time in the reaction. Therefore, the following experiments were designed to investigate in detail.

3.3. Evolution of the Surface Sulfate Species. It was reported in the previous studies that NH_4^+ in ABS could react with NO under a reaction atmosphere, and the remaining SO_4^{2-} would combine with the metal ions in catalyst to form thermally stable metal sulfates.[30] Hence, the Me-p-5 h sample was then taken as an example to implement the NO + O_2 TPSR test. As presented in Figure 3a, the outlet NO concentration did not fall below the saturation value at the beginning for all samples until the temperature exceeded a certain point. As temperature continued to rise, the outlet NO concentration returned slowly to the initial saturation value. Strikingly, a scarce NH_3 signal emerged throughout the TPSR test, which meant that almost all NH_4^+ in the ABS was consumed by NO + O_2, followed by the reaction: NH_4HSO_4 + NO + O_2 → N_2 + H_2O + H_2SO_4.

Differences among the three reactions could be further elaborated from the temperature at which NO consumption reached the maximum. Followed by the order of Fe-p-5 h (~180 °C) ≈ Ce-p-5 h (~180 °C) < Mn-p-5 h (~390 °C), such sequence manifested that the difficulty of NH_4^+ in ABS to participate in the reaction was different among three samples. The harder the NH_4^+ was to participate in the reaction, the

https://doi.org/10.1021/acs.jpcc.2c02233
J. Phys. Chem. C 2022, 126, 12168–12177

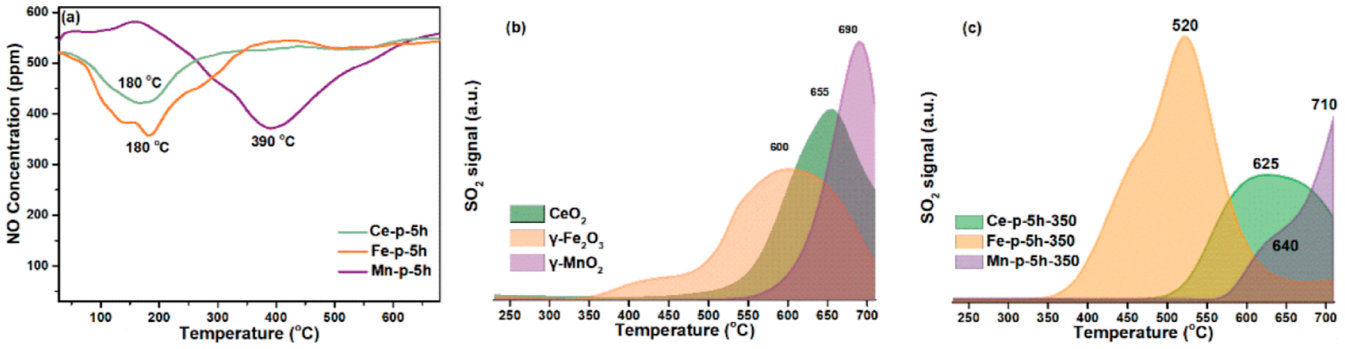

Figure 3. (a) NO + O_2 TPSR results of Me-p-5 h. (b) SO_2-TPD results of CeO_2, γ-Fe_2O_3, and γ-MnO_2 and (c) NH_3-TPSR profiles of the Me-p-5h-350.

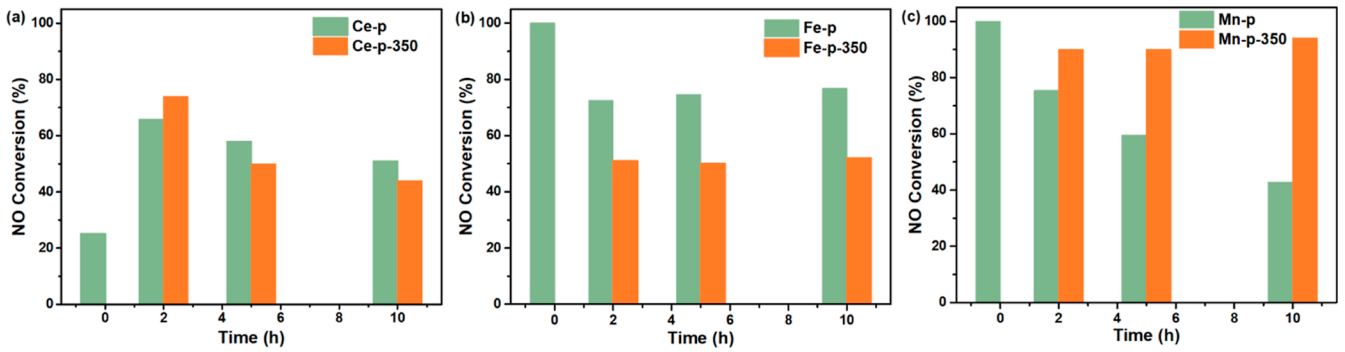

Figure 4. NO conversion of Me-p-2/5/10 h, Me-p-2/5/10 h-350, and fresh samples at 250 °C.

larger the ABS accumulated, which also identified with what the IC test obtained.

Conclusions can be drawn that the deposited ABS could be consumed by NO + O_2 while being constantly generated, and thus the equilibrium between deposition and consumption of ABS was well established. Moreover, the NH_4^+ in ABS on Ce-p-5 h and Fe-p-5 h could participate in the reaction at a relatively lower temperature, while the NH_4^+ in ABS on Mn-p-5 h seemed less reactive in such a reaction. Also, it perhaps illustrated that ABS may have less effect on long-running sulfurization for CeO_2 and γ-Fe_2O_3, but for γ-MnO_2, ABS would exert a more obvious inhibitory effect on its activity.

The thermal stability and reactivity of metal sulfates species initially mentioned in TG was further measured in SO_2-TPD. As displayed in Figure 3b, all samples showed a strong desorption peak at about 600 °C, which could be attributed to the decomposition of metal sulfates formed by the strong interaction between SO_2 and metal elements in the catalyst.[23] Differently, γ-Fe_2O_3 possessed a weak desorption peak at about 420 °C, which was assigned to the desorption of SO_2 adsorbed on surface.[34] Followed by the order of $Fe_2(SO_4)_3$ (~600 °C) < $Ce_2(SO_4)_3$ (~655 °C) < $MnSO_4$ (~690 °C), an identical result with NO-TPSR's could be acquired from the desorption peak temperature of CeO_2, γ-Fe_2O_3, and γ-MnO_2.[23] More precisely, ΔG_f of corresponding metal sulfates of CeO_2, γ-Fe_2O_3, and γ-MnO_2 at 250 °C (Table S1) declared the spontaneous formation of three metal sulfates. $MnSO_4$ was the easiest to form and existed most stably among them, which is in line with the SO_2-TPD results.

As can be noticed, the increased rate of metal sulfates in IC slowed down with time. Taking CeO_2 as an example, the accumulation rate of $Ce_2(SO_4)_3$ was 1.16 wt %·h^{-1} in 2−5 h, while this value was merely 0.46 wt %·h^{-1} in 5−10 h (calculated), showing a sharp decline. There was a report[35] that showed that metal sulfates could be consumed by NH_3 reduction at around 250 °C, so NH_3-TPSR over Me-p-5h-350 was implemented to disclose the reactivity of these metal sulfates (Figure 3c). As the system beings heating up after the adsorption of NH_3 reached saturation at ambient temperature, the SO_2 desorption signal was gradually observed. Compared with SO_2-TPD (Figure 3b), the desorption peak temperature of SO_2 all obviously moved toward lower points; thus, it's reasonable to deduce that the bonding of SO_4^{2-} and metal ions was weakened when NH_3 presented, and an easier SO_2 escape was succeeded therefore. Relevant studies corroborated above inference and gave the product in the reaction. Yu et al.[36] investigated the deSO_x mechanism of Mn oxides, and they found that the oxidized sulfur species would favor the formation of ABS instead of $MnSO_4$, generated from introduced NH_3. Ma et al.[31] directly observed the reaction of NH_3 with $Ce_2(SO_4)_3$ and verified ABS formation by first principles calculations. Jangjou et al.[37] alleged that NH_3 could drive S-containing species from a seemingly more strongly adsorbed position/form to the less stable ABS.

Conclusions can be drawn that the formed metal sulfates could be consumed by NH_3 while being constantly generated and became another source of ABS thereby. Moreover, $Fe_2(SO_4)_3$ could participate in the reaction relatively easily, while $Ce_2(SO_4)_3$ and $MnSO_4$ seemed less reactive in such a reaction according to the SO_2 escape temperature. Also, it perhaps illustrated why γ-Fe_2O_3 possessed the least amount of surface metal sulfate after sulfurization, followed by CeO_2 and γ-MnO_2.

3.4. Effect of Sulfate Species on the Sulfur Tolerance.

The effect of sulfate species formed on the surface of catalysts during the sulfur tolerance test would be intuitively uncovered

https://doi.org/10.1021/acs.jpcc.2c02233
J. Phys. Chem. C 2022, 126, 12168−12177

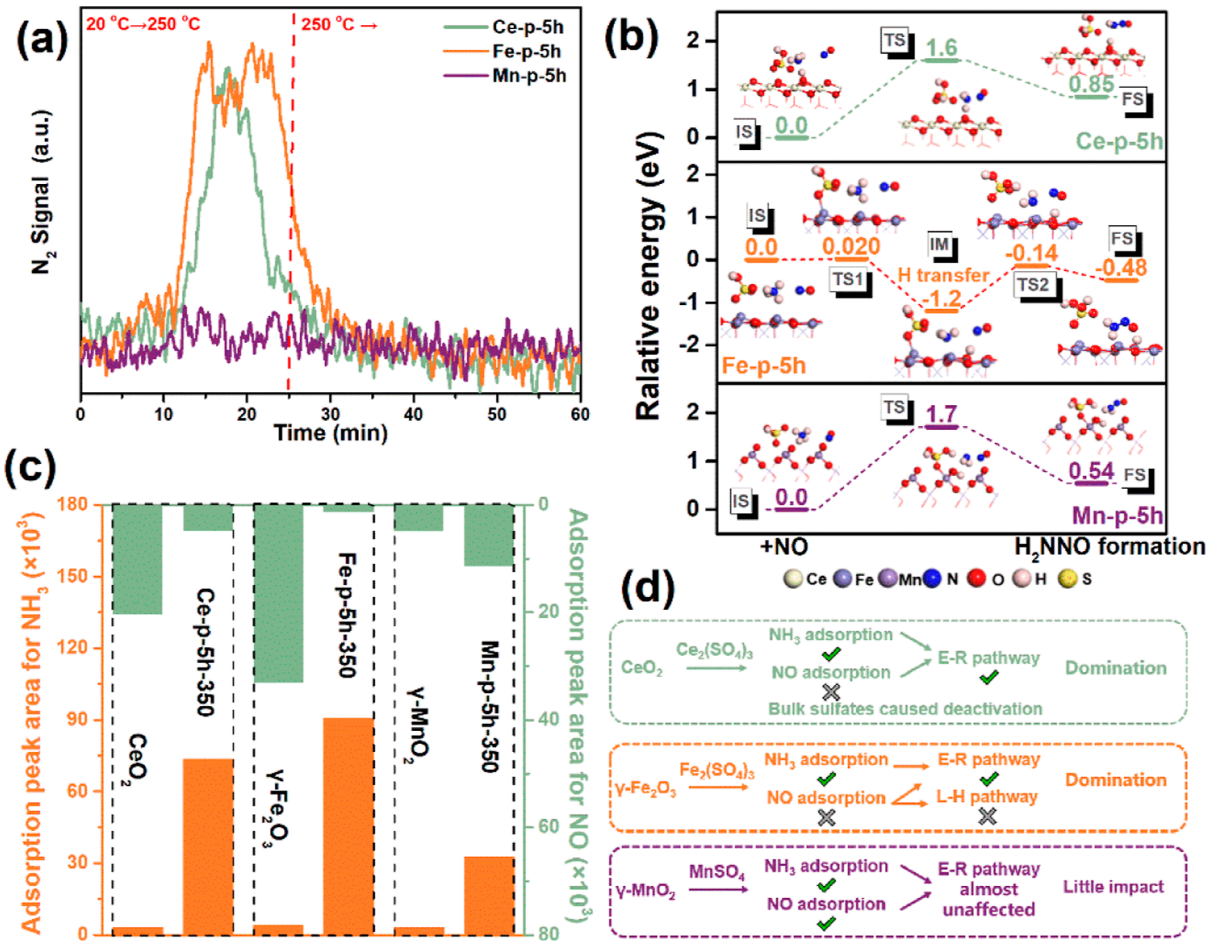

Figure 5. (a) NO + O_2 TPSR results of Me-p-5 h at 250 °C. (b) Theoretical energy and structure profiles for the reaction of NO with deposited ABS over Me-p-5 h. (c) Adsorption peak area of fresh and Me-p-5 h-350 for NH_3/NO at 20 °C. (d) Flow chart unfolding the effect of metal sulfates on the reaction mechanism.

when we combined two types of activity data together (Figure 4). Descriptively, histograms (the red one) were made by the activity data of each sample at the initial state, 2nd, 5th, and 10th h of the sulfur tolerance test, in which both ABS and metal sulfate species presented. Then, a sample with only metal sulfates on its surface was obtained through high-temperature treatment of the sample after the sulfur tolerance test, in which complete decomposition of ABS was guaranteed. Afterward, the catalytic performance of the obtained Me-p-2/5/10 h-350 samples at 250 °C were plotted as histograms (the blue one). Highlighting the differences in the catalytic performance among the Me-p-2/5/10 h, Me-p-2/5/10 h-350, and fresh samples, the weight of two sulfate species could be visually revealed: For CeO_2 and γ-Fe_2O_3, before and after removing the surface ABS, the catalytic activity (represented by the red and green histograms) had basically the same trend over time. That is to say that the residual ABS hardly affected the activity due to its dynamic equilibrium between deposition and consumption. While the catalytic performance of γ-MnO_2 almost returned to the level before sulfurization after removing ABS, and its activity recovery degree remained nearly unchanged with the SO_2 poisoning time. Thus, (1) for CeO_2 and γ-Fe_2O_3, their sulfur tolerance is mainly determined by metal sulfates,[25−27] benefiting from ABS consumed in time; (2) while for γ-MnO_2, $MnSO_4$ formed did not play a significant role, the coverage effect of deposited ABS was speculated to make more contribution to the continuous downward sulfur tolerance.

3.5. Coverage Effect of Deposited ABS and the Working Mechanism of Metal Sulfates. The coverage effect of the deposited ABS on γ-MnO_2, which was distinctive from CeO_2 and γ-Fe_2O_3, needed more direct evidence for being self-proven, and so TPSR was further investigated (Figure 5a) to disclose the reactivity of these surface-deposited ABS. After the adsorption of NO + O_2 reached saturation at ambient temperature, the Me-p-5 h were heated up to 250 °C at a rate of 10 °C·min^{-1} and held for several hours to record the N_2 signal. For Ce-p-5 h and Fe-p-5 h, on account of the swift reaction between NO + O_2 and NH_4^+ in ABS, the deposited ABS was easily consumed by NO and produced N_2. However, scarcely any N_2 signal emerged on Me-p-5 h, proving the quite inert NH_4^+ in deposited ABS on γ-MnO_2. Besides, the SCR performance of the Mn-s-2/5/10 h at 250 °C could be another supporting argument (Figure S3). Few differences were recognized among the catalytic activity of the fresh γ-MnO_2, Mn-p-2/5/10 h-350, and the Mn-s-2/5/10 h at 250 °C, consolidating the weak influence of $MnSO_4$.

Furthermore, the reaction pathways of the ABS with NO on the surface of each Me-p-5 h were simulated by computational methods. It's known that NH_3 can be effectively adsorbed on Brønsted acid sites of the catalyst, and then the NH_3-SCR reaction takes place following the commonly accepted E-R

https://doi.org/10.1021/acs.jpcc.2c02233
J. Phys. Chem. C 2022, 126, 12168−12177

reaction mechanism. Therein, the adsorbed NH_3 reacts with the gas phase NO to form H_2NNO, which can rapidly decompose to N_2 and H_2O. The formation of H_2NNO is identified as the rate-determining step.[38] Such a reaction route is universal when it comes to the reaction of NO with the deposited ABS.[40] Here, the initial energy of ABS on each Me-p-5 h was deemed as 0.00 eV. As shown in Figure 5b, the SO_4^{2-} of ABS was tightly bound to the Me−O−Me site of the Me-p-5 h through a close chemical bond formed between the S atom and the surface O atoms. When a NO molecule approached the NH_4^+ of ABS, the NH_4^+ was then activated by transferring an H^+ to HSO_4^- to form electrically neutral H_2SO_4 and an H to the adjacent Ce/Fe/Mn site, leading to the formation of an H_2NNO intermediate (IM) through the bonding of the two N atoms. This intermediate was never seen and, therefore, probably underwent rapid decomposition to yield the reaction products, N_2 and H_2O.[38] On the surface of CeO_2 and γ-MnO_2, the migrations of H^+ from NH_4^+ to O in HSO_4^- and H from NH_4^+ to O in the adjacent Ce/Mn site were a synergistic one-step process. However, on the surface of γ-Fe_2O_3, the migration of H and H^+ split into two steps due to a new stable intermediate (IM) formed, attributing to the ultralow energy barrier of H migration from NH_4^+ to O in the adjacent Fe site (TS1). The energy barrier for the formation of H_2NNO in the above reaction was 1.60 eV for CeO_2 (from 0.00 to 1.60 eV), 1.06 eV for γ-Fe_2O_3 (from −1.20 to −0.14 eV), and 1.71 eV for γ-MnO_2 (from 0.00 to 1.70 eV), respectively. The higher energy barrier of γ-MnO_2 implied that the reaction between ABS and NO on it was difficult to carry out, which was consistent with the experimental results. Therefore, the coverage effect of the deposited ABS on γ-MnO_2 that gave rise to the poor sulfur tolerance was thoroughly verified.

Known from the above discussion, the difference in the decomposition ability of ABS would lead to the diversity in its coverage effect. Besides, metal sulfates seemed to directly determine the sulfur tolerance of CeO_2 and γ-Fe_2O_3, whereas they show less impact on γ-MnO_2. An essential reason for these phenomena was expected to be acquired. Hence the effect of metal sulfates on the adsorption of reactant molecules was investigated first, and corresponding results are shown in Figure S4. More intuitively, the adsorption peak area of each sample for the above two reaction molecules at ambient temperature is placed in Figure 5c. The metal sulfates formed on the surface of the catalyst were confirmed to bring abundant acid sites, manifested by a significant increase in the amount of adsorbed NH_3 on Me-p-5 h-350. Such an increase might be derived from hydroxyl-like groups provided by S═O from SO_4^{2-}, which were highly related to the generation of more Brønsted acid sites.[41] On the contrary, the NO adsorption on Ce/Fe-p-5 h-350 was obviously reduced compared with what their fresh one exhibited, demonstrating that the adsorption and oxidation of NO were immensely inhibited. This was because the oxygen atom which could be used to bridge NO and Ce/Fe cation was covered by SO_4^{2-} after sulfation.[41] Compared with CeO_2 and γ-Fe_2O_3, the adsorption behavior of NO on γ-MnO_2 was completely different; a slightly enhanced state, which indicated that $MnSO_4$ promoted the adsorption of NO species. This could probably also be the reason for the difference between the effect of manganese sulfate and other metal sulfates on the activity. Consequently, such radical changes on the adsorption behavior of NH_3/NO molecules would be bound to exert an influence on the progress of the SCR reaction mechanism. Therefore, further exploration of the effect of metal sulfates on the reaction mechanism was inevitable.

The in situ DRIFTS spectra of the NH_3-SCR reaction on CeO_2, γ-Fe_2O_3, and γ-MnO_2 at 250 °C are given in Figure S5a−c. Also, to simulate the surface that had been undergoing the sulfur tolerance test for several hours, CeO_2, γ-Fe_2O_3, and γ-MnO_2 were impelled to preadsorb SO_2 + O_2 at 250 °C for about 1 h and collected as a spectral background, respectively, with the spectra of the NH_3-SCR reaction on sulfated CeO_2, γ-Fe_2O_3 and γ-MnO_2 at 250 °C given in Figure S5d−f. A detailed description of the change in in situ DRIFTS spectra is placed in the Supporting Information. Related conclusions explained the difference in the effects of different metal sulfates on the activity, and a flow chart in Figure 5dis attached for clarity:

(1) γ-Fe_2O_3: As the published study,[26] the $Fe_2(SO_4)_3$ species formed inhibited the NO adsorption and thus cut off the Langmuir−Hinshelwood (L−H) reaction pathway, leading to a cliff activity drop. It then switched on the Eley−Rideal (E−R) reaction pathway later and made an enhancement in the SCR efficiency.

(2) γ-MnO_2: The SCR reaction over γ-MnO_2 and sulfated γ-MnO_2 both proceeded through the E−R reaction mechanism. $MnSO_4$ species did increase its surface acidity and facilitate NH_3 adsorption to a certain extent, while the simultaneously increased NO adsorption was not conducive to the E−R pathway (gaseous NO preferred). Meanwhile, the deposited nitrates may cover the active sites and block the pore structure, resulting in NH_3 adsorption suppression and a further decrease in the denitrification activity.[42,43] Thus, the promotion effect was offset, and surface metal sulfates show little impact on its activity.

(3) CeO_2: The E−R reaction pathway remained despite the sulfation. Therefore, it's definable that its catalytic performance was promoted significantly at first, generating from an increased NH_3 adsorption due to the enhanced surface acidity and suppressed NO adsorption. However, bulk sulfates formed later were proved by IR results, so the gradual decline brought about by those poor-activity bulk sulfates covering on CeO_2 was predictable.[27] NH_3-TPD profiles in Figure S6 verified the effect of bulk sulfates by characterizing the change in the desorption peak area before and after H_2O washing.[39] Obviously, all desorption peaks of Ce-p-10h-350-H_2O moved to a low temperature. It was evident that the elimination of bulk sulfates over sulfated Ce-p-10h-350 was beneficial to the exposure of NH_3 adsorbed on weak acid sites (peak α and β). Also, such weak acid sites were proved to play a crucial role in the NH_3-SCR activity.[40]

3.6. Schematic of the Evolution Mechanism of Sulfur-Containing Species. According to the qualitative and quantitative characterization results of the surface sulfate species and their reaction characteristics with the feed gas NH_3/NO, a dynamic evolution during the reaction process is proposed in Scheme 1. It can be seen that eqs 3 and 4 represent the deposition of ABS and metal sulfate, and eqs 5 and 6 represent their decomposition process, meaning the simultaneous existence of deposition and decomposition of these surface sulfur-containing species. The scheme uncovers

https://doi.org/10.1021/acs.jpcc.2c02233
J. Phys. Chem. C 2022, 126, 12168−12177

Scheme 1. Dynamic Evolution Process of the Surface Sulfate Species[a]

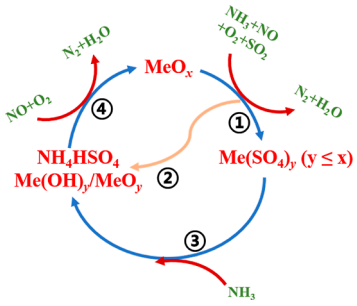

[a]The indicators ①, ②, ③, and ④ represent the reactions shown in eqs 3−6 in the text.

that the fundamental reason for the deactivation of different metal oxide catalysts in a sulfur-containing atmosphere is closely related to the difference in the deposition/decomposition ability of these surface sulfate species.

$$①:\ MeO_x + SO_2 + O_2 \rightarrow Me(SO_4)_y \quad (3)$$

$$②:\ NH_3 + SO_2 + O_2 + H_2O \rightarrow NH_4HSO_4 \quad (4)$$

$$③:\ Me(SO_4)_y + NH_3 + H_2O \rightarrow Me(OH)_y + NH_4HSO_4 \quad (5)$$

$$④:\ NH_4HSO_4 + NO + O_2 \rightarrow N_2 + H_2O + H_2SO_4$$
$$Me(OH)_y + O_2 \rightarrow MeO_x + H_2O \quad (6)$$

In detail, reactions ① and ② (eqs 3 and 4) represent the formation of surface sulfate species on the catalyst in a SO_2-containing reaction. First, the metal oxide catalyst (MeO_x) oxidizes the gaseous SO_2 to SO_3 and is itself reduced to the low-valence oxide (MeO_y) ($y \leq x$). Then, the generated SO_3 can continue to react with MeO_y to form $Me(SO_4)_y$ or react with NH_3 to form ABS. In other words, reactions ① and ② are competing processes. Besides, unstable sulfite will be rapidly oxidized to sulfates (e.g., $FeSO_4 \rightarrow Fe_2(SO_4)_3$),[44] and other stable sulfates remain unchanged (e.g., $Ce_2(SO_4)_3$ and $MnSO_4$).[23,31,32] Therefore, the deposited metal sulfate is generally referred to as $Me(SO_4)_y$ ($y \leq x$). For different metal oxides, the generation ability of surface sulfate species is also different. Also, in this system, the formation order was $MnSO_4 > Ce_2(SO_4)_3 > Fe_2(SO_4)_3$, given by SO_2-TPD.

Similar to the reaction of metal sulfate and ammonia, the surface metal sulfate $Me(SO_4)_y$ ($y \leq x$) can react with the adsorbed NH_3 and H_2O to form a microdomain liquid phase reaction and then to generate $Me(OH)_y$ and ABS, as shown in reaction ③ (eq 5).[31,36,37] Generally speaking, for a double replacement reaction, the solubility product (K_{sp}) of the hydroxide precipitation, as shown in Table S2, determines the reaction progress. The smaller the K_{sp}, the easier the reaction. As a result, $Me(SO_4)_y$ ($y \leq x$) is more likely to participate in the order of $Fe_2(SO_4)_3 > Ce_2(SO_4)_3 > MnSO_4$, supported by the results of IC and NH_3-TPSR. This also answers the reason why some catalysts such as γ-Fe_2O_3 and MnO_x/CeO_2(NR) and so forth can maintain long-term stability even after the continuous generation of metal sulfate species, which could inhibit the redox property of the catalysts.[26,31]

For reaction ④ (eq 6), two reactions are included. One is the ABS consumption, proved by the NO-TPSR reaction and IC results. Here, the order of difficulty on different metal oxide catalysts is $CeO_2 > \gamma$-$Fe_2O_3 > \gamma$-MnO_2. This means that for γ-MnO_2, there is no dynamic equilibrium between deposition and decomposition of the surface ABS, and the surface covering effect is the nature of the continuous decrease in its activity.

The other reaction is the decomposition of insoluble hydroxide, $Me(OH)_y$, which finally generates stable MeO_x under the atmosphere of O_2, completing the metal oxide cycle. Consequently, due to the different intrinsic properties of different metal oxides, the difficulty of each step in the cycle is also different, which will affect or even ultimately determine the sulfur tolerance of the catalyst to a large extent.

4. CONCLUSIONS

In summary, key determinants behind the sulfur tolerance of CeO_2, γ-Fe_2O_3, and γ-MnO_2 were weighed, and their working mechanism was expressly illuminated. Given the analysis of the sulfate species formed and their reaction characteristics in the reaction atmosphere, it was found that:

(1) The reactivity of NH_4^+ was a decisive factor in determining whether the ABS coverage effect worked. In this paper, the inert NH_4^+ in the deposited ABS on γ-MnO_2 made the coverage effect the main cause for its poor sulfur tolerance. While for CeO_2 and γ-Fe_2O_3, their lifetime in SO_2 were mainly determined by the effect of metal sulfates, benefiting from timely consumption of ABS promoted by active NH_4^+.

(2) NH_3 was well competent for facilitating the breakdown of metal sulfates, the difficulty of which was another factor affecting the sulfur tolerance of metal oxide catalysts. The easier the reaction, such as γ-Fe_2O_3, the better it can maintain its catalytic performance in a sulfur-containing atmosphere.

(3) A dynamic evolution during the reaction process was proposed, and a certain guiding significance was presented. Attention should be paid to the mutual restriction and interaction between the reaction atmosphere and surface species when developing novel low-temperature SO_2-tolerance catalysts.

■ ASSOCIATED CONTENT

Supporting Information

The Supporting Information is available free of charge at https://pubs.acs.org/doi/10.1021/acs.jpcc.2c02233.

Computational details, XRD patterns, TG curves, ΔG_f, NO conversion comparison of γ-MnO_2, NH_3/NO-TPD profiles, in situ DRIFTS spectra, NH_3-TPD profiles, and K_{sp} (PDF)

■ AUTHOR INFORMATION

Corresponding Authors

Jingfang Sun − *Jiangsu Key Laboratory of Vehicle Emissions Control, Center of Modern Analysis, Nanjing University, Nanjing, Jiangsu 210093, P. R. China;* orcid.org/0000-0003-1963-4874; Email: sunjf@nju.edu.cn

Dan Li − *Key Laboratory of Green Chemistry and Technology, Ministry of Education, College of Chemistry, Sichuan University, Chengdu, Sichuan 610064, P. R. China;* orcid.org/0000-0003-4433-649X; Email: danli@scu.edu.cn

https://doi.org/10.1021/acs.jpcc.2c02233
J. Phys. Chem. C 2022, 126, 12168−12177

Authors

Dongqi An − *Key Laboratory of Mesoscopic Chemistry of MOE, School of Chemistry and Chemical Engineering and Jiangsu Key Laboratory of Vehicle Emissions Control, Nanjing University, Nanjing, Jiangsu 210093, P. R. China*

Shan Yang − *Collaborative Innovation Center of Functionalized Probes for Chemical Imaging in Universities of Shandong, Shandong Provincial Key Laboratory of Clean Production of Fine Chemicals, College of Chemistry, Chemical Engineering and Materials Science, Shandong Normal University, Jinan, Shandong 250014, P. R. China*

Weixin Zou − *Jiangsu Key Laboratory of Vehicle Emissions Control, School of Environment, Nanjing University, Nanjing, Jiangsu 210093, P. R. China*

Wei Tan − *Key Laboratory of Mesoscopic Chemistry of MOE, School of Chemistry and Chemical Engineering and Jiangsu Key Laboratory of Vehicle Emissions Control, Nanjing University, Nanjing, Jiangsu 210093, P. R. China*

Jiawei Ji − *Key Laboratory of Mesoscopic Chemistry of MOE, School of Chemistry and Chemical Engineering and Jiangsu Key Laboratory of Vehicle Emissions Control, Nanjing University, Nanjing, Jiangsu 210093, P. R. China*

Qing Tong − *Jiangsu Key Laboratory of Vehicle Emissions Control, Center of Modern Analysis, Nanjing University, Nanjing, Jiangsu 210093, P. R. China*

Chuanzhi Sun − *Collaborative Innovation Center of Functionalized Probes for Chemical Imaging in Universities of Shandong, Shandong Provincial Key Laboratory of Clean Production of Fine Chemicals, College of Chemistry, Chemical Engineering and Materials Science, Shandong Normal University, Jinan, Shandong 250014, P. R. China;* orcid.org/0000-0002-3744-9800

Lin Dong − *Key Laboratory of Mesoscopic Chemistry of MOE, School of Chemistry and Chemical Engineering and Jiangsu Key Laboratory of Vehicle Emissions Control, School of Environment, Center of Modern Analysis, Nanjing University, Nanjing, Jiangsu 210093, P. R. China;* orcid.org/0000-0002-8393-6669

Complete contact information is available at: https://pubs.acs.org/10.1021/acs.jpcc.2c02233

Notes

The authors declare no competing financial interest.

■ ACKNOWLEDGMENTS

The financial support from the National Natural Science Foundation of China (nos. 21972062, 21976081, 21976111) is gratefully acknowledged.

■ REFERENCES

(1) Twigg, M. V. Progress and Future Challenges in Controlling Automotive Exhaust Gas Emissions. *Appl. Catal., B* **2007**, *70*, 2−15.

(2) Doronkin, D. E.; Benzi, F.; Zheng, L.; Sharapa, D. I.; Amidani, L.; Studt, F.; Roesky, P. W.; Casapu, M.; Deutschmann, O.; Grunwaldt, J.-D. NH_3-SCR over V-W/TiO_2 Investigated by Operando X-ray Absorption and Emission Spectroscopy. *J. Phys. Chem. C* **2019**, *123*, 14338−14349.

(3) Yao, X.; Ma, K.; Zou, W.; He, S.; An, J.; Yang, F.; Dong, L. Influence of preparation methods on the physicochemical properties and catalytic performance of MnO-CeO_2 catalysts for NH_3-SCR at low temperature. *Chin. J. Catal.* **2017**, *38*, 146−159.

(4) Chen, J.; Chen, Y.; Zhou, M.; Huang, Z.; Gao, J.; Ma, Z.; Chen, J.; Tang, X. Enhanced Performance of Ceria-Based NO_x Reduction Catalysts by Optimal Support Effect. *Environ. Sci. Technol.* **2017**, *51*, 473−478.

(5) Kang, L.; Han, L.; He, J.; Li, H.; Yan, T.; Chen, G.; Zhang, J.; Shi, L.; Zhang, D. Improved NO_x Reduction in the Presence of SO_2 by Using Fe_2O_3-Promoted Halloysite-Supported CeO_2-WO_3 Catalysts. *Environ. Sci. Technol.* **2019**, *53*, 938−945.

(6) Li, L.; Li, P.; Tan, W.; Ma, K.; Zou, W.; Tang, C.; Dong, L. Enhanced low-temperature NH_3-SCR performance of CeTiO catalyst via surface Mo modification. *Chin. J. Catal.* **2020**, *41*, 364−373.

(7) Busca, G.; Lietti, L.; Ramis, G.; Berti, F. Chemical and Mechanistic Aspects of the Selective Catalytic Reduction of NO_x by Ammonia over Oxide Catalysts: A Review. *Appl. Catal., B* **1998**, *18*, 1−36.

(8) Hu, H.; Cai, S.; Li, H.; Huang, L.; Shi, L.; Zhang, D. Mechanistic Aspects of deNO_x Processing over TiO_2 Supported Co-Mn Oxide Catalysts: Structure-Activity Relationships and In Situ DRIFTs Analysis. *ACS Catal.* **2015**, *5*, 6069−6077.

(9) Zhang, L.; Shi, L.; Huang, L.; Zhang, J.; Gao, R.; Zhang, D. Rational Design of High-Performance deNO_x Catalysts Based on $Mn_xCo_{3-x}O_4$ Nanocages Derived from Metal−Organic Frameworks. *ACS Catal.* **2014**, *4*, 1753−1763.

(10) Xu, H.; Yan, N.; Qu, Z.; Liu, W.; Mei, J.; Huang, W.; Zhao, S. Gaseous Heterogeneous Catalytic Reactions over Mn-Based Oxides for Environmental Applications: A Critical Review. *Environ. Sci. Technol.* **2017**, *51*, 8879−8892.

(11) Yan, L.; Liu, Y.; Zha, K.; Li, H.; Shi, L.; Zhang, D. Scale-Activity Relationship of MnO_x-FeO_y Nanocage Catalysts Derived from Prussian Blue Analogues for Low-Temperature NO Reduction: Experimental and DFT Studies. *ACS Appl. Mater. Interfaces* **2017**, *9*, 2581−2593.

(12) Wang, H.; Qu, Z.; Dong, S.; Xie, H.; Tang, C. Superior Performance of $Fe_{1-x}W_xO_\delta$ for the Selective Catalytic Reduction of NO_x with NH_3: Interaction between Fe and W. *Environ. Sci. Technol.* **2016**, *50*, 13511−13519.

(13) Shan, W.; Song, H. Catalysts for the selective catalytic reduction of NOx with NH_3 at low temperature. *Catal. Sci. Technol.* **2015**, *5*, 4280−4288.

(14) Liu, F.; He, H. Structure−Activity Relationship of Iron Titanate Catalysts in the Selective Catalytic Reduction of NO_x with NH_3. *J. Phys. Chem. C* **2010**, *114*, 16929−16936.

(15) Maier, S. M.; Jentys, A.; Janousch, M.; van Bokhoven, J. A.; Lercher, J. A. Unique Dynamic Changes of Fe Cationic Species under NH_3-SCR Conditions. *J. Phys. Chem. C* **2012**, *116*, 5846−5856.

(16) Tang, C.; Zhang, H.; Dong, L. Ceria-based catalysts for low-temperature selective catalytic reduction of NO with NH_3. *Catal. Sci. Technol.* **2016**, *6*, 1248−1264.

(17) Shan, W.; Liu, F.; He, H.; Shi, X.; Zhang, C. A superior Ce-W-Ti mixed oxide catalyst for the selective catalytic reduction of NO_x with NH_3. *Appl. Catal., B* **2012**, *115-116*, 100−106.

(18) Yu, C.; Huang, B.; Dong, L.; Chen, F.; Yang, Y.; Fan, Y.; Yang, Y.; Liu, X.; Wang, X. Effect of Pr/Ce addition on the catalytic performance and SO_2 resistance of highly dispersed MnO_x/SAPO-34 catalyst for NH_3-SCR at low temperature. *Chem. Eng. J.* **2017**, *316*, 1059−1068.

(19) Gan, L.; Li, K.; Yang, W.; Chen, J.; Peng, Y.; Li, J. Core-shell-like structured α-MnO_2@CeO_2 catalyst for selective catalytic reduction of NO: Promoted activity and SO_2 tolerance. *Chem. Eng. J.* **2020**, *391*, 123473.

(20) Ali, S.; Li, Y.; Zhang, T.; Bakhtiar, S. u. H.; Leng, X.; Li, Z.; Yuan, F.; Niu, X.; Zhu, Y. Promotional effects of Nb on selective catalytic reduction of NO with NH_3 over Fe_x-$Nb_{0.5-x}$-$Ce_{0.5}$ (x = 0.45, 0.4, 0.35) oxides catalysts. *Mol. Catal.* **2018**, *461*, 97−107.

(21) Xie, C.; Sun, Y.; Zhu, B. The promoting mechanism of doping Mn, Co, and Ce on gas adsorption property and anti-SO_2 oxidation over γ-Fe_2O_3 (001) surface: A density functional theory study. *Colloids Surf., A* **2021**, *628*, 127218.

(22) Fan, Z.; Shi, J.-W.; Niu, C.; Wang, B.; He, C.; Cheng, Y. The insight into the role of Al_2O_3 in promoting the SO_2 tolerance of

MnO_x for low-temperature selective catalytic reduction of NO_x with NH_3. *Chem. Eng. J.* **2020**, *398*, 125572.
(23) Wang, Y.; Yi, W.; Yu, J.; Zeng, J.; Chang, H. Novel Methods for Assessing the SO_2 Poisoning Effect and Thermal Regeneration Possibility of MO_x-WO_3/TiO_2 (M = Fe, Mn, Cu, and V) Catalysts for NH_3-SCR. *Environ. Sci. Technol.* **2020**, *54*, 12612−12620.
(24) He, G.; Gao, M.; Peng, Y.; Yu, Y.; Shan, W.; He, H. Superior Oxidative Dehydrogenation Performance toward NH_3 Determines the Excellent Low-Temperature NH_3-SCR Activity of Mn-Based Catalysts. *Environ. Sci. Technol.* **2021**, *55*, 6995−7003.
(25) Tan, W.; Liu, A.; Xie, S.; Yan, Y.; Shaw, T. E.; Pu, Y.; Guo, K.; Li, L.; Yu, S.; Gao, F.; et al. Ce-Si Mixed Oxide: A High Sulfur Resistant Catalyst in the NH_3-SCR Reaction through the Mechanism-Enhanced Process. *Environ. Sci. Technol.* **2021**, *55*, 4017−4026.
(26) Yu, Y.; Tan, W.; An, D.; Wang, X.; Liu, A.; Zou, W.; Tang, C.; Ge, C.; Tong, Q.; Sun, J.; et al. Insight into the SO_2 resistance mechanism on γ-Fe_2O_3 catalyst in NH_3-SCR reaction: A collaborated experimental and DFT study. *Appl. Catal., B* **2021**, *281*, 119544.
(27) Zhang, L.; Zou, W.; Ma, K.; Cao, Y.; Xiong, Y.; Wu, S.; Tang, C.; Gao, F.; Dong, L. Sulfated Temperature Effects on the Catalytic Activity of CeO_2 in NH_3-Selective Catalytic Reduction Conditions. *J. Phys. Chem. C* **2015**, *119*, 1155−1163.
(28) Wu, Z.; Jin, R.; Wang, H.; Liu, Y. Effect of ceria doping on SO_2 resistance of Mn/TiO_2 for selective catalytic reduction of NO with NH_3 at low temperature. *Catal. Commun.* **2009**, *10*, 935−939.
(29) Jin, R.; Liu, Y.; Wang, Y.; Cen, W.; Wu, Z.; Wang, H.; Weng, X. The role of cerium in the improved SO_2 tolerance for NO reduction with NH_3 over Mn-Ce/TiO_2 catalyst at low temperature. *Appl. Catal., B* **2014**, *148-149*, 582−588.
(30) Guo, K.; Zhu, Y.; Yan, Z.; Liu, A.; Du, X.; Wang, X.; Tan, W.; Li, L.; Sun, J.; Tong, Q.; et al. The dual effects of ammonium bisulfate on the selective catalytic reduction of NO with NH_3 over Fe_2O_3-WO_3 catalyst confined in MCM-41. *Chem. Eng. J.* **2020**, *389*, 124271.
(31) Ma, Z.; Sheng, L.; Wang, X.; Yuan, W.; Chen, S.; Xue, W.; Han, G.; Zhang, Z.; Yang, H.; Lu, Y.; Wang, Y. Oxide Catalysts with Ultrastrong Resistance to SO_2 Deactivation for Removing Nitric Oxide at Low Temperature. *Adv. Mater.* **2019**, *31*, 1903719.
(32) Zhang, L.; Li, L.; Cao, Y.; Yao, X.; Ge, C.; Gao, F.; Deng, Y.; Tang, C.; Dong, L. Getting insight into the influence of SO_2 on TiO_2/CeO_2 for the selective catalytic reduction of NO by NH_3. *Appl. Catal., B* **2015**, *165*, 589−598.
(33) Tsungyu, L.; Hsunling, B. Metal Sulfate Poisoning Effects over MnFe/TiO_2 for Selective Catalytic Reduction of NO by NH_3 at Low Temperature. *Ind. Eng. Chem. Res.* **2018**, *57*, 4848−4858.
(34) Chen, L.; Li, R.; Li, Z.; Yuan, F.; Niu, X.; Zhu, Y. Effect of Ni Doping in $Ni_xMn_{1-x}Ti_{10}$ (x = 0.1-0.5) on Activity and SO_2 resistance for NH_3-SCR of NO Studied with in Situ DRIFTS. *Catal. Sci. Technol.* **2017**, *7*, 3243−3257.
(35) Mu, J.; Li, X.; Wang, X.; Fan, S.; Yin, Z.; Li, Z.; Tadé, M. O.; Liu, S. New Insight into the Effects of NH_3 on SO_2 Poisoning for in Situ Removal of Metal Sulfates in Low-Temperature NH_3-SCR over an Fe-V Catalyst. *J. Phys. Chem. C* **2020**, *124*, 21396−21406.
(36) Yu, S.; Lu, Y.; Cao, Y.; Wang, J.; Sun, B.; Gao, F.; Tang, C.; Dong, L. Composite Catalytic Systems: A Strategy for Developing the Low Temperature NH_3-SCR Catalysts with Satisfactory SO_2 and H_2O Tolerance. *Catal. Today* **2019**, *327*, 235−245.
(37) Jangjou, Y.; Wang, D.; Kumar, A.; Li, J.; Epling, W. S. SO_2 Poisoning of the NH_3-SCR Reaction over Cu-SAPO-34: Effect of Ammonium Sulfate versus Other S-Containing Species. *ACS Catal.* **2016**, *6*, 6612−6622.
(38) Topsøe, N.-Y. Mechanism of the Selective Catalytic Reduction of Nitric Oxide by Ammonia Elucidated by in Situ On-Line Fourier Transform Infrared Spectroscopy. *Science* **1994**, *265*, 1217−1219.
(39) Wang, X.; Du, X.; Liu, S.; Yang, G.; Chen, Y.; Zhang, L.; Tu, X. Understanding the Deposition and Reaction Mechanism of Ammonium Bisulfate on a Vanadia SCR catalyst: A Combined DFT and Experimental Study. *Appl. Catal., B* **2020**, *260*, 118168.
(40) Wei, L.; Cui, S.; Guo, H.; Ma, X.; Zhang, L. DRIFT and DFT study of cerium addition on SO_2 of Manganese-based Catalysts for low temperature SCR. *J. Mol. Catal. A: Chem.* **2016**, *421*, 102−108.
(41) Yang, S.; Guo, Y.; Chang, H.; Ma, L.; Peng, Y.; Qu, Z.; Yan, N.; Wang, C.; Li, J. Novel effect of SO_2 on the SCR reaction over CeO_2: Mechanism and significance. *Appl. Catal., B* **2013**, *136-137*, 19−28.
(42) Wei, L.; Cui, S.; Guo, H.; Ma, X.; Wan, Y.; Yu, S. The mechanism of the deactivation of MnO_x/TiO_2 catalyst for low-temperature SCR of NO. *Appl. Surf. Sci.* **2019**, *483*, 391−398.
(43) Liu, J.; Liu, J.; Zhao, Z.; Wei, Y.; Song, W.; Li, J.; Zhang, X. A Unique Fe/Beta@TiO_2 Core-Shell Catalyst by Small-Grain Molecular Sieve as the Core and TiO_2 Nanosize Thin Film as the Shell for the Removal of NO_x. *Ind. Eng. Chem. Res.* **2017**, *56*, 5833−5842.
(44) Wermink, W. N.; Versteeg, G. F. The Oxidation of Fe(II) in Acidic Sulfate Solutions with Air at Elevated Pressures. Part 2. Influence of H_2SO_4 and Fe(III). *Ind. Eng. Chem. Res.* **2017**, *56*, 3789−3796.

https://doi.org/10.1021/acs.jpcc.2c02233
J. Phys. Chem. C 2022, 126, 12168−12177